Photo-Ablation of Human Vitreous Opacities by Light-Induced Vapor Nanobubbles

Félix Sauvage[1], Juan C. Fraire[1], Katrien Remaut[1], J. Sebag[2,3], Karen Peynshaert[1], Michael Harrington[4], Frans J. Van de Velde[5], Ranhua Xiong[1], Marie-José Tassignon[6], Toon Brans[1], Kevin Braeckmans[1] and Stefaan C. De Smedt[1*]

[1]Lab. General Biochemistry & Physical Pharmacy, Faculty of Pharmaceutical Sciences, Ghent University, Ottergemsesteenweg 460, Ghent, Belgium

[2]VMR Institute for Vitreous Macula Retina, Huntington Beach, CA, USA

[3]Doheny Eye Institute /UCLA, Los Angeles, CA, USA

[4]Huntington Medical Research Institutes, Pasadena, CA, USA

[5]Schepens Eye Research Institute, Harvard Medical School, Boston, MA, USA

[6]Department of Ophthalmology, Antwerp University Hospital, University of Antwerp, Belgium

*Corresponding author: Stefaan.desmedt@ugent.be

Abstract

Myopia, diabetes and aging are the main causes of progressive vitreous collagen aggregation, resulting in vitreous opacities which can significantly disturb vision. As vitreous opacities, which induce the visual phenomenon of 'floaters', are accessible with nanomaterials and light, we propose a nanotechnology-based approach to locally ablate them with highly reduced light energy compared to the more traditional YAG laser therapy. Our strategy relies on the plasmon properties of gold nanoparticles that generate vapor nanobubbles upon pulsed-laser illumination whose mechanical force can ablate vitreous opacities. We designed gold nanoparticles coated with hyaluronic acid which have excellent diffusional mobility in human vitreous, an essential requirement to reach the vitreous opacities. In addition, we found that HA-coated gold nanoparticles can accumulate extensively on human vitreous opacities which were obtained by vitrectomy from patients with vision degrading myodesopsia. When subsequently applying

nanosecond laser pulses, the collagen aggregates were efficiently destroyed with ~1000 times less light energy as typically used in YAG laser therapy. This low energy ‘floater-specific destruction’, which is due to the accumulation of the small gold nanoparticles on the opacities, is attractive as it may be safer to the surrounding ocular tissues while at the same time being easier and faster to apply compared to YAG laser therapy where the opacities need to be ablated piece by piece by a tightly focused laser beam. Gold nanoparticle assisted photo-ablation may therefore provide a safer, faster and more reliable destruction of vitreous opacities in the treatment of ophthalmologic diseases.

Keywords: vitreous floaters, ophthalmology, pulsed-laser, gold nanoparticles, collagen fibers, collagen aggregates

Graphical abstract (TOC)

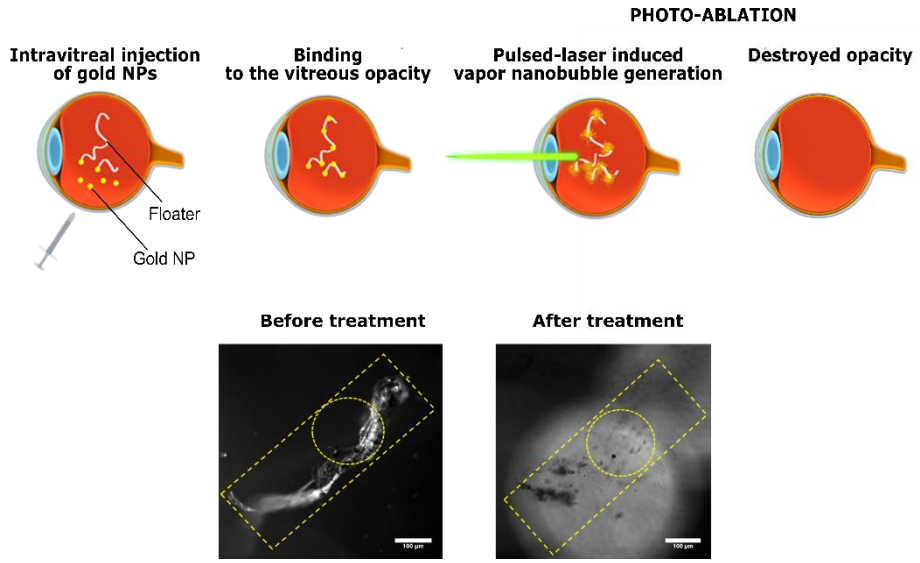

Proteins are important in living organisms, as they are involved in structural functions and play a role in many physiological processes. In some situations, misfolded or unfolded proteins can accumulate and form toxic biological aggregates which are involved in many diseases, such as amyloid diseases (Alzheimer's disease, Parkinson disease…).[1] While huge challenges remain to reach and treat amyloid aggregates in the brain, pathological aggregates also arise in other locations of the body that are more easily accessible to physical stimuli and advanced materials. In this investigation we focus on protein aggregates which form in the vitreous body of the human eye (Figure 1A). Vitreous is a colorless transparent gel mostly composed of water, collagen and negatively charged hyaluronic acid (HA).[2] The collagen strands ('fibrils') and HA chains form a biomolecular network that confers gelatinous solidity to the vitreous body. However, in myopia and with aging, the vitreous body is increasingly liquefied due to structural changes in the biopolymer network and depolymerization of HA, resulting in collagen aggregation[2]. This destabilization of the vitreous body and concurrent dehiscence of vitreo-retinal adhesion often result in acute posterior vitreous detachment and the sudden appearance of 'floaters' which disturb vision due to light scattering by the dense collagen matrix. Many patients suffering from vitreous floaters often complain of a significantly negative impact on their quality of life.[3,4] All too often, patients with vitreous floaters are left untreated. However, recent advances have made available two therapeutic options: (i) pars plana vitrectomy, *i.e.* the surgical removal of the patient's vitreous and its replacement by a saline solution,[5–7] or (ii) a non-invasive treatment of the vitreous opacities with a neodymium yttrium garnet laser (Nd:YAG).[8]

The principle behind YAG laser therapy is that locally applied laser pulses (typically 2-8 mJ per pulse; up to 1000 shots per floater) result in plasma production and 'optical breakdown' that may disrupt vitreous opacities.[9,10] In 2002, a retrospective study indicated however that only

38% of patients treated with YAG laser found a moderate improvement in their symptoms, showing that YAG laser therapy is far from optimal,[11,12] as confirmed in more recent studies.

Furthermore, it is known that YAG laser therapy is not completely safe. Indeed, cases of cataract,[13] open-angle glaucoma [14] and posterior lens capsule rupture [15] have been reported. Clearly, while treatment of biological aggregates in the vitreous with YAG lasers is an attractive approach, significant room for improvement remains. For instance, it is generally considered that the shape, size and location of the aggregates in the vitreous can have a detrimental impact on the YAG laser treatment efficacy, thereby necessitating a trial and error approach based on the practitioner's observation and judgement.[16,17] Therefore, technological improvements are needed that allow to photoablate vitreous collagen aggregates, no matter their size, shape or location, while being safe and easier to perform.

Considering this clear clinical need, we developed a nanotechnology-based approach for more efficient photo-ablation of micro- and macroscopic opacities in human vitreous. In particular we rely on the surface plasmon properties of gold nanoparticles (AuNPs) which tremendously enhance laser light absorption.[18,19] Upon pulsed-laser illumination (typically nanosecond laser pulses), AuNPs are quickly heating up to several hundred degrees. Consequently, the water of the surrounding environment evaporates to form vapor nanobubbles (VNBs) emerging around the surface of the AuNP (Figure 1B).[18,20] Such VNBs will first expand and then collapse thereby generating high-pressure shockwaves. As illustrated in Figure 1C, we hypothesized that VNBs would allow to mechanically destroy opacities in the vitreous if AuNPs can be targeted to those opacities upon intravitreal injection, a well-accepted administration route to deliver (biological) drugs in the eye. We first explored our hypothesis making use of 'artificial vitreous opacities' *i.e.* collagen fiber bundles obtained through heating of type I collagen solutions. We investigated (i) the intrinsic capacity of nanobubbles to break collagen fibers dispersed in water and (ii) the capacity of AuNPs functionalized with hyaluronic acid to diffuse in bovine vitreous and bind to collagen fibers. Subsequently, we tested the concept of gold nanoparticle assisted

photo-ablation on human vitreous obtained after vitrectomy in patients with vision degrading myodesopsia.

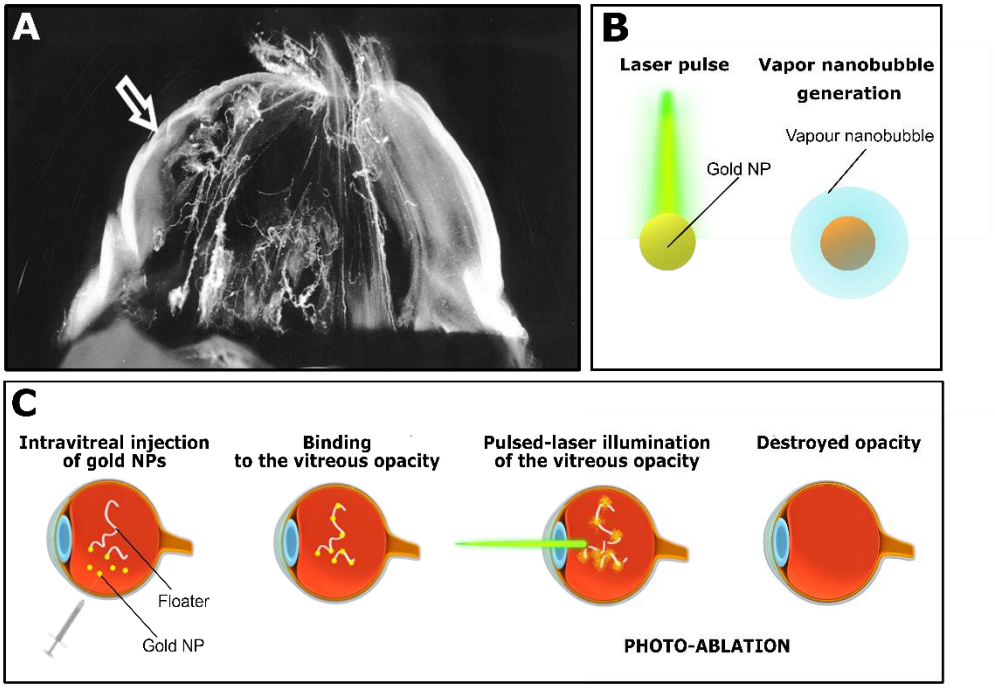

Figure 1. (A) Dark-field microscopy of vitreous in an 88 year-old patient shows age-related aggregation of vitreous collagen into visible fibers in the central vitreous body that induce vision-disturbing floaters. The dense collagen matrix of the outer vitreous body (arrow) also induces floaters after separation from the retina (posterior vitreous detachment). With permission from [21]. (B) Schematic representation of the generation of vapor nanobubbles (VNBs) from gold nanoparticles (AuNPs) illuminated with a pulsed-laser. (C) Schematic representation of the concept 'gold nanoparticle assisted photo-ablation': upon intravitreal injection AuNPs bind to the opacities; subsequent pulsed-laser illumination locally generates vapor nanobubbles which mechanically destroy the vitreous opacities.

Results/Discussion

Nanobubbles generated from cationic AuNPs (cat-AuNPs) can break collagen fibers

First, we evaluated if laser induced nanobubbles have the capacity to break artificially made collagen fibers. Collagen fibers were prepared through heating of type I collagen solutions. As Figure 2A shows, the collagen solution turned turbid upon heating at 37 °C, indicating the formation of collagen fibers (insert ii). These fibers in water were subsequently labeled with Col-F, a fluorescent probe which stains collagen and elastin.[22] The presence of collagen fibers could be confirmed by dark field and fluorescence microscopy, an example of which is given in Figure 2B. As the dark field microscopy images in Figure 2C show, cat-AuNPs of 70 nm spontaneously bound to the collagen fibers. Figure 2D shows a dark field microscopy image of a collagen fiber carrying cat-AuNPs respectively before, during and after applying a single laser pulse of 200 µJ (~1.1 J/cm²); immediately after the laser pulse VNBs (which scatter laser light) can be observed on the fiber as bright spots.

As Figure 2E and F indicate, a single laser pulse of either 200 µJ or 600 µJ (corresponding to a laser fluence of 1.1 and 3.3 J/cm², respectively) was not sufficient to break the collagen fibers. However, an 800 µJ laser pulse (~ 4.5 J/cm²) did affect the size of the collagen fibers, while the size of the fibers could be reduced further by applying more laser pulses (Figure 2G).

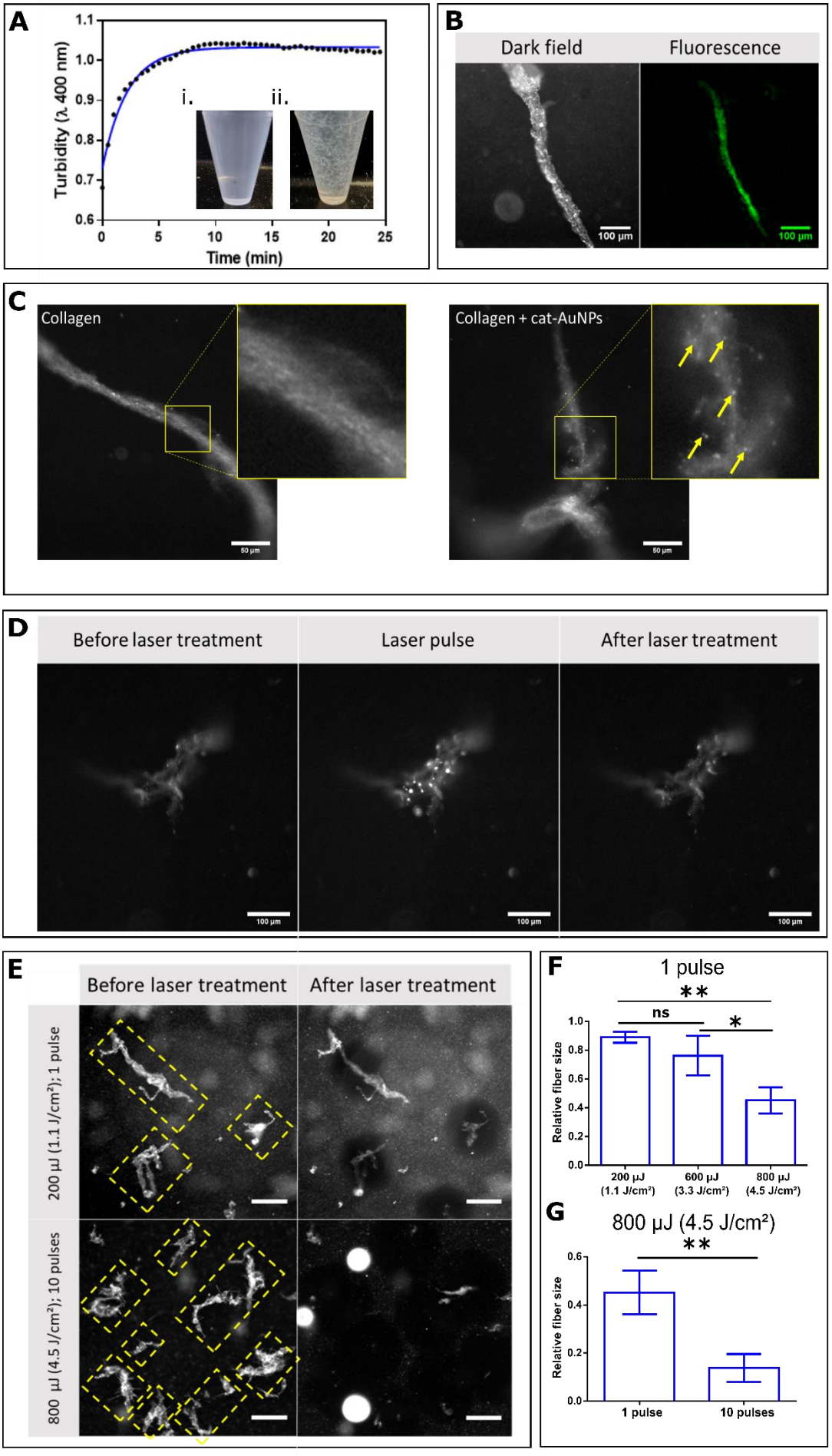
A
Turbidity (λ 400 nm)
Time (min)
i.
ii.
B
Dark field
Fluorescence
100 µm
C
Collagen
Collagen + cat-AuNPs
D
Before laser treatment
Laser pulse
After laser treatment
E
Before laser treatment
After laser treatment
200 µJ (1.1 J/cm²); 1 pulse
800 µJ (4.5 J/cm²); 10 pulses
F
1 pulse
ns
*
**
Relative fiber size
200 µJ (1.1 J/cm²)
600 µJ (3.3 J/cm²)
800 µJ (4.5 J/cm²)
G
800 µJ (4.5 J/cm²)
**
Relative fiber size
1 pulse
10 pulses

Figure 2. (A) Turbidity change of a collagen solution indicating the formation of collagen fibers. Inserts correspond to respectively a solution of collagen (i) and a dispersion of collagen fibers (ii). (B) Representative dark field and fluorescence microscopy images of a Col-F stained collagen fiber (in water) carrying 70 nm cat-AuNPs. (C) Representative images of collagen fibers (in water) before and after treatment with cat-AuNPs. The presence of cat-AuNPs on the collagen fibers can be appreciated in the right insert. (D) Dark field microscopy images of a collagen fiber carrying cat-AuNPs (10^{10} particles/ml) respectively before, during and after applying a single laser pulse of 200 µJ (~1.1 J/cm²): during the laser pulse VNBs (which reflect the laser light) can be observed on the fiber as bright spots. (E) Representative images of collagen fibers (in water) before and after treatment with nanobubbles; either a single pulse of 200 µJ (~1.1 J/cm²) or 10 pulses of 800 µJ (~4.5 J/cm²) were applied. The yellow dotted squares/rectangles indicate the position of the fibers. The scale bar in E is 100 µm. (F, G) Relative size of the collagen fibers upon treating the fibers under various conditions: the intensity (E; one laser pulse) or the number of laser pulses (F; 800 µJ; ~4.5 µJ/cm²) were varied. In all experiments the laser beam was focused on the center of the fibers. Fiber length was determined from the microscopy images using ImageJ software. Data are shown as mean +/- SD. Statistical significance: student's t-test, * indicates $p<0.05$, ** indicates $p<0.01$, ns indicates non-significant.

Coating of AuNPs with negatively charged HA prevents their immobilization in vitreous

Clearly, to allow binding of AuNPs to opacities in vitreous, the AuNPs should not become immobilized at the injection spot but remain sufficiently mobile to be able to reach the fibers which may be a distance away from the injection spot. Upon injection of cat-AuNPs in bovine vitreous, we noticed they got immobilized. Dark field images revealed binding of the cat-AuNPs to the vitreous network (Figure 3A). These observations are in agreement with earlier data from us and others [23,24] which showed the immobilization of cationic polystyrene nanoparticles and cationic liposomes in vitreous. This is highly likely attributed to the anionic nature of the vitreous hyaluronan facilitating interactions with positively charged nanoparticles.[25,26]

As we have demonstrated before that coating of nanoparticles with negatively charged hyaluronic acid (HA) can restore their mobility in vitreous, [23,25–27] we synthesized hyaluronic acid-coated AuNPs (HA-AuNPs). The zeta-potential (ZP) of cat-AuNPs (in water) was + 39 mV while it turned to -18 mV for HA-AuNPs (Figure 3B), confirming the coating of the gold nanoparticles with HA.

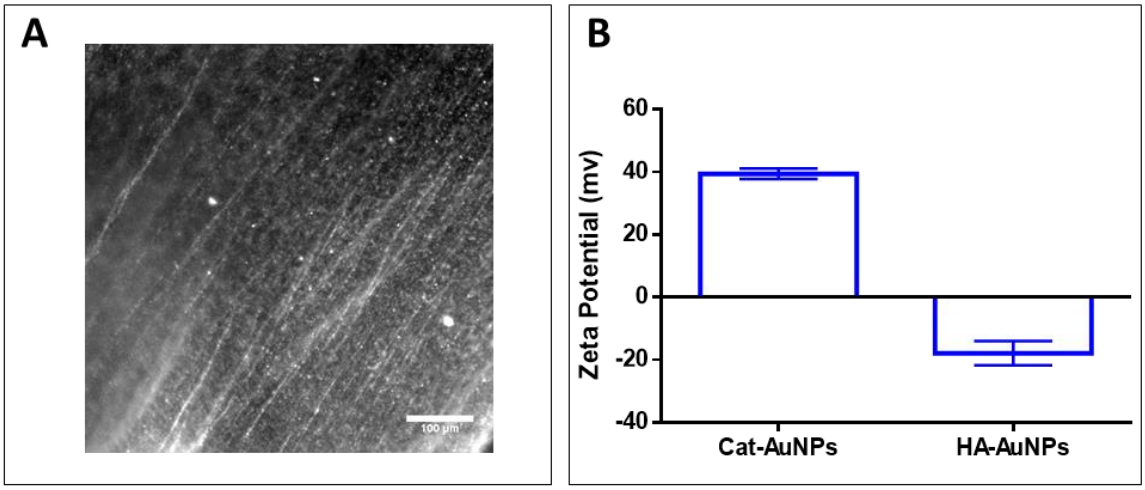

Figure 3. (A) Dark field microscopy images of 70 nm cat-AuNPs in bovine vitreous show their immobilization on the collagen strands of the vitreous. (B) Zeta potential measurements of Cat-AuNPs and HA-AuNPs in water.

To confirm whether HA coating of the AuNPs indeed avoids their obstruction in vitreous we used scattering recovery after fragmentation (SRAF), as explained in detail in the experimental section. Figure 4 shows a representative SRAF experiment on HA-AuNPs dispersed in water. The dark field microscopy image in the outmost left panel shows the scattered light by the gold NPs in suspension. Applying a single laser pulse in the indicated circular region causes the AuNPs to become fragmented, which locally reduces the intensity of the scattered light. Due to diffusion, intact AuNPs from the surrounding area gradually move into this fragmented zone, resulting in a gradual recovery of the light scattering intensity (Figure 4; right panel). The diffusion coefficient of the HA-AuNPs in water (as calculated from the recovery curve) was estimated to be around 3.2 +/- 0.1 $\mu m^2/s$, which is fairly close to the D-value as measured by nanoparticle tracking analysis (NTA), being 4.7 +/-0.8 $\mu m^2/s$ (data not shown). The fact that SRAF underestimates the diffusion coefficient is likely due to the simplified semi-quantitative

method that we used to calculate it from the scattering recovery curve. Nevertheless, it is sufficiently reliable for our purpose, which is to verify if HA-AuNPs have better mobility in vitreous as compared to cat-AuNPs (see below).

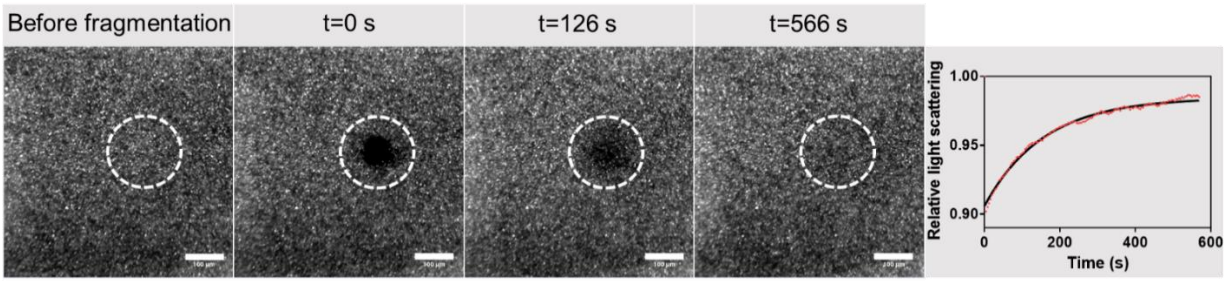

Figure 4. SRAF measurements on HA-AuNPs in water. Dark field microscopy images of a suspension of HA-AuNPs (70 nm) in water before, during (t = 0 s) and after (t > 0 s) fragmentation of the HA-AuNPs in the fragmentation zone (which is indicated by the dotted circle; 100 µm in diameter). To fragment the HA-AuNPs a single 7 nanosecond laser pulse (200 µJ; ~1.1 J/cm²) was applied. The light scattering recovery curve is shown in the right panel (see Movie S1); the relative light scattering in the Y-axes is the light scattering as measured at a certain time point (in the fragmentation zone) divided by the light scattering measured (in the fragmentation zone) before fragmentation. The red symbols are the experimental data; the black line is the fitted curve. For movies, see supplementary material.

Figure 5 shows the outcome of SRAF measurements on respectively cat-AuNPs and HA-AuNPs injected in bovine vitreous. Clearly, the nearly complete absence of light scattering recovery in the fragmentation zone (Figure 5, top panel) confirms that cat-AuNPs are mostly stuck in vitreous. Instead, HA-AuNPs have much better mobility in bovine vitreous (Figure 5, lower panel), with a diffusion coefficient (1.9 +/- 0.4 µm²/s) somewhat lower than in water, as could

be expected due to the presence of the biopolymer network in the vitreous.

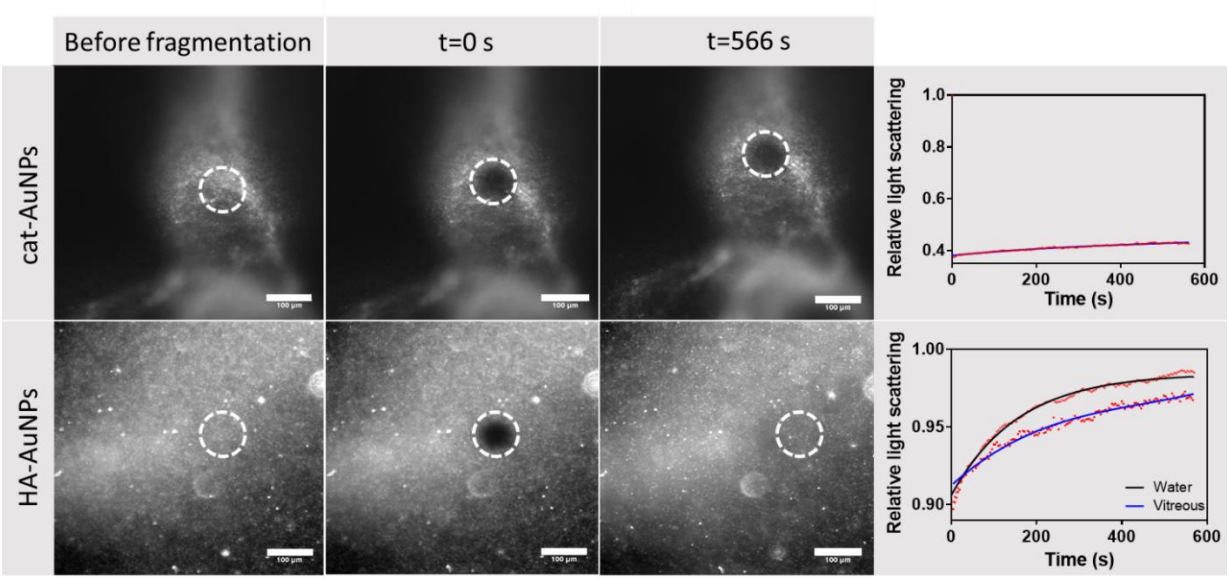

Figure 5. SRAF measurements on HA-AuNPs in bovine vitreous. (A) Dark field microscopy images of cat-AuNPs (70 nm) and HA-AuNPs (70 nm) injected in bovine vitreous before and after fragmentation. The scale bar is 100 µm. To fragment the HA-AuNPs a single 7 nanosecond laser pulse (200 µJ; ~1.1 J/cm²) was applied. The dotted circle indicates the fragmentation zone (around 100 µm diameter). As the panel at the right shows, while there was is no light scattering recovery for the cat-AuNPs (see also Movie S2) recovery clearly occurred for HA-AuNPs (see also Movie S3). The relative light scattering in the Y-axes of the panels at the right is the light scattering as measured at a certain time point (in the fragmentation zone) divided by the light scattering measured (in the fragmentation zone) before fragmentation. The red symbols are the experimental data; the lines represent the fitted curves. For movies, see supplementary material.

Nanobubbles generated from (70 nm) HA-AuNPs allow to break collagen fibers

To evaluate whether AuNPs, when coated with HA, bind collagen fibers and keep their capacity to break fibers (as seen with cat-AuNPs, Figure 2), HA-AuNPs were mixed with artificial collagen fibers dispersed in water. Figure 6 (top panel) shows that collagen fibers remain unaffected when exposed to a single 800 µJ (~4.5 J/cm²) laser pulse only (*i.e.* without treating them with HA-AuNPs). With a single laser pulse of 200 µJ (~1.1 J/cm²), collagen fibers 'carrying' HA-AuNPs (note the accumulation of the HA-AuNPs on the fibers) were again poorly affected. Instead, when the intensity of the (single) laser pulse was increased up to 800

μJ (4.5 J/cm²), collagen fibers carrying HA-AuNPs became clearly broken (bottom panel) in agreement with the results obtained with cat-AuNPs (Figure 2).

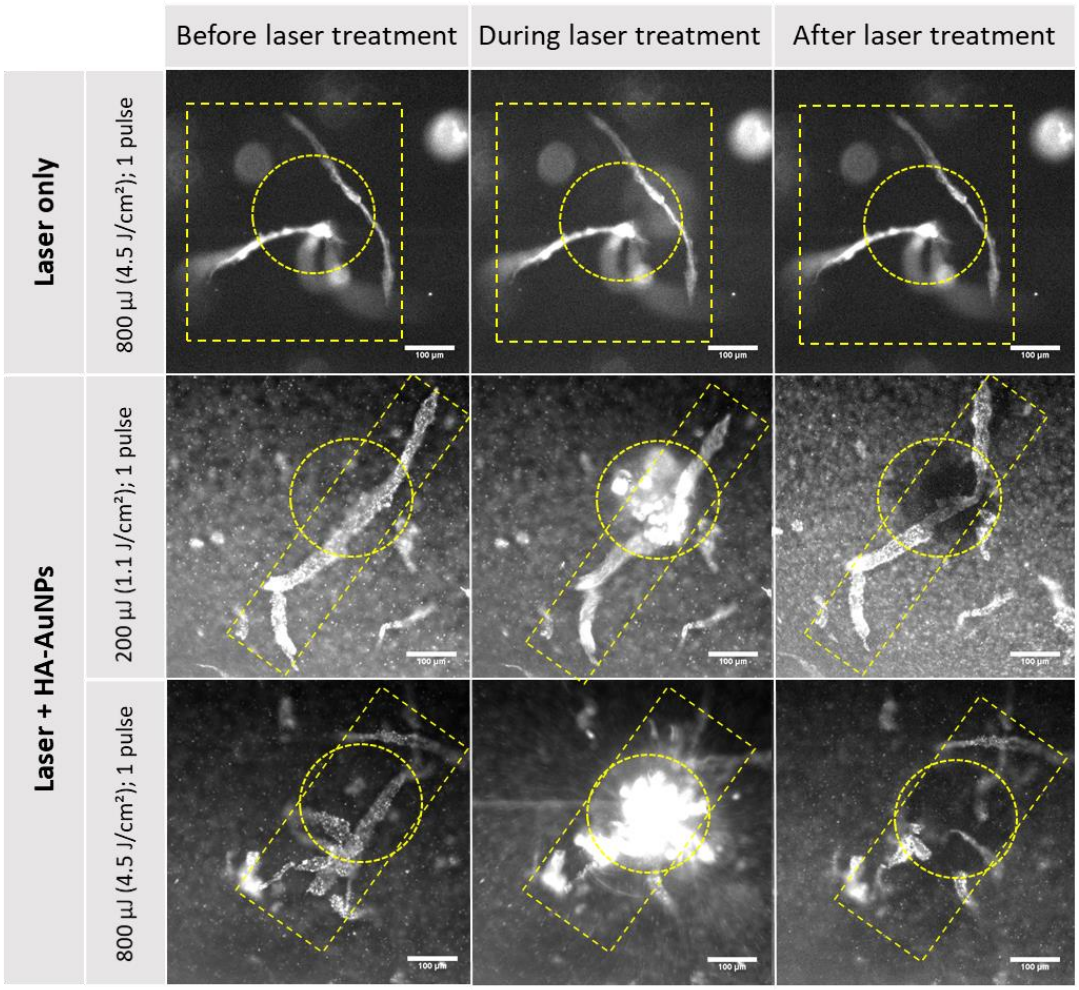

Figure 6. Dark field microscopy images of collagen fibers (dispersed in water) respectively before, during and after applying a single laser pulse of different intensities. In the top row HA-AuNPs were not added while in the middle and bottom rows HA-AuNPs (70 nm; 10^{10} NPs/ml) were attached to the collagen fibers; the scale bar is 100 µm. The yellow dotted squares/rectangles indicate the position of the targeted fiber. Dotted circles indicate the position of the laser beam. During laser treatment (merged) vapor nanobubbles can be appreciated as bright spots (middle panel in the second and third row).

Binding of 'small' AuNPs (10 nm) to collagen fibers

Clearly, the approach to break collagen fibers by laser light induced VNBs conceptually works when using 70 nm AuNPs. However, as evident from the dark field microscopy images, such fairly large AuNPs quite strongly scatter light. Strong scattering of light by intravitreally

injected nanoparticles would be highly undesirable as it might lower the visual acuity of the patient. Instead, it is well-known that light scattering is much weaker for smaller gold nanoparticles from which, however, VNBs are not easily formed.[28] Yet, it has been reported before that it is still possible to generate VNB when those small AuNPs locally agglomerate to form effectively larger particle clusters,[42] as already shown to happen at the surface of cells.[43] Seeing that HA-AuNPs did bind to collagen fibers (which is a form of local agglomeration), we subsequently studied whether or not smaller HA-AuNPs (*i.e.* 10 nm instead of 70 nm) still allow to form VNB and destroy the collagen fibers.

First, we studied the binding of 10 nm HA-AuNPs (ZP=-22.1 +/-1.62 mV) to collagen fibers. As shown in Figure 7 A and B, TEM images confirmed the binding of small HA-AuNPs to collagen fibers with a density of approximately 45 NPs/μm^2 and 250 NPs/μm^2 when incubated at 10^{10} and 10^{12} NPs/ml, respectively. Figure 7C shows experimentally measured UV-VIS extinction spectra of respectively collagen fibers alone, HA-AuNPs in water (10^{12} NPs/ml) and HA-AuNPs bound to collagen fibers (10^{12} NPs/ml). It can be appreciated that at a concentration of 10^{12} NPs/ml, once the AuNPs bind to collagen fibers, a red shift of the maximum of the localized surface plasmon resonance (LSPR) peak occurs from 521 nm to 534 nm, indicative of particle clustering (plasmon coupling).

The insert of panel C in Figure 7 shows photographs of (i) a collagen fiber suspension, (ii) a suspension of small HA-AuNPs (10^{12} NPs/ml) and (iii) a suspension of collagen fibers in the presence of small HA-AuNPs. The red color of the collagen fibers in presence of AuNPs (insert iii) is related to the binding of the AuNPs on the fibers, in agreement with the TEM images (Figure 7A and B) and red-shift of the extinction spectrum.

To further confirm that the observed red-shift is due to particle clustering, in Figure 7 E and F we simulated the extinction spectra of respectively 10 nm AuNPs dispersed in water (non-clustered; Figure 7D) and of 10 nm AuNPs attached to collagen fibers (in water) at a density of respectively 45 NPs/μm^2 (Figure 7E) and 250 NPs/μm^2 (Figure 7F). The simulations were

performed as reported previously by Fraire *et al.*.[44] The simulated extinction spectrum of free 10 nm AuNPs in water (Figure 7D) had a peak at 521 nm, matching very well to the 522 nm peak that we found experimentally. At a density of 45 NPs/μm^2 a red-shift occurred to 528 nm (Figure 7E), which became 532 nm at a density of 250 NPs/μm^2 (Figure 7F). This matches again very well with the experimentally observed extinction peak at 534 nm, providing further evidence that the HA-AuNPs cluster upon binding to the collagen fibers.

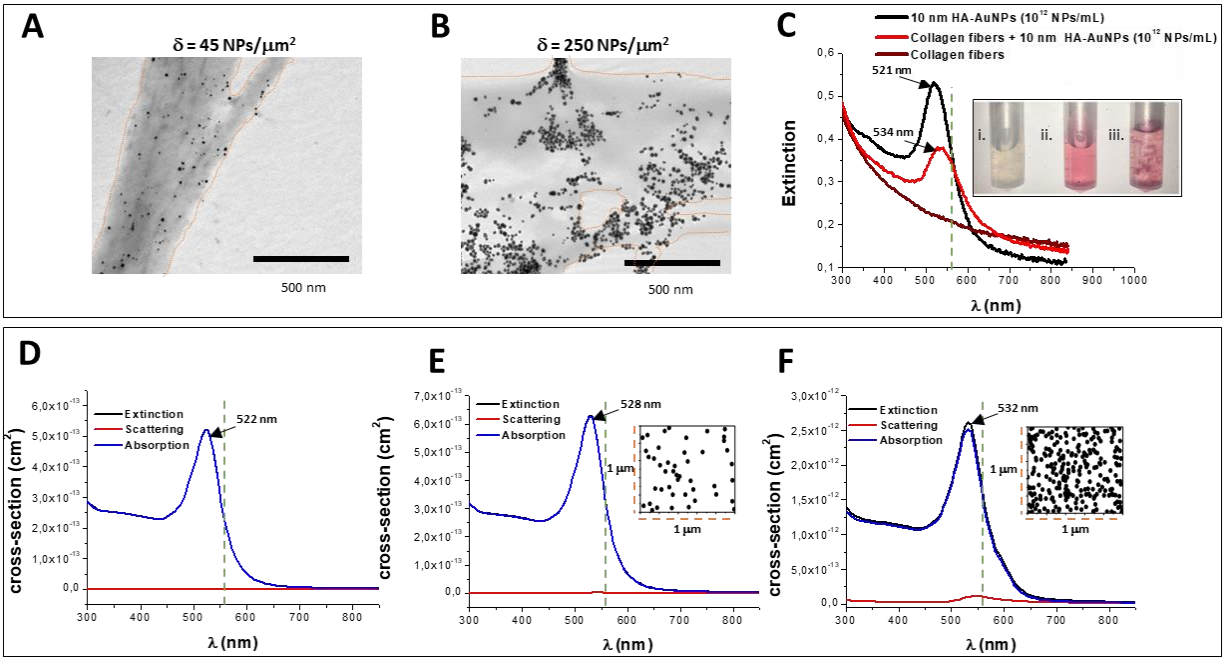

Figure 7. (A, B) Representative TEM images of collagen fibers (in water) carrying a lower (A; 45 NPs/μm²; 10^{10} NPs/ml) or higher (B; 250 NPs/μm²; 10^{12} NPs/ml) amount of HA-AuNPs. (C) Experimentally measured UV-vis spectra of 10 nm HA-AuNPs dispersed in water (black) and added to a dispersion of collagen fibers (red: 10^{12} NPs/ml). The insert shows a suspension of collagen fibers in water (i), HA-AuNPs in water (ii) and added to a dispersion of collagen fibers (iii). (D) Simulated optical response of 10 nm AuNPs dispersed in water (*i.e.* non-clustered) and of collagen fibers (in water) carrying the 10 nm AuNPs at a density of (E) 45 NPs/μm^2 (as in A) and (F) 250 NPs/μm^2 (as in B). Note that in (D) and (E) the extinction and absorption completely overlap. For more details on the simulations of the optical responses we refer to the experimental section.

Photo-ablation of collagen fibers with 10 nm HA-AuNPs

Subsequently we evaluated whether or not (i) vapor nanobubbles could still be generated from the 10 nm HA-AuNPs upon clustering to collagen fibers and (ii) if such nanobubbles allow to break collagen fibers dispersed in water or bovine vitreous.

First, we noticed (Figure 8 A and B) that with 10 nm HA-AuNPs in water it was far more difficult to observe the formation of vapor nanobubbles, when compared to the 70 nm gold NPs. This size dependency was indeed expected [41] since at the laser fluences used in our study 10 nm sized HA-AuNPs are too small to generate VNBs. The few VNBs observed at a laser fluence of around 3 J/cm² (Figure 8B) are most likely generated by some aggregated HA-AuNPs. Figure 8 C and D show that applying a single laser pulse (800 µJ; ~4.5 J/cm²) to HA-AuNPs dispersed in bovine vitreous (10^{12} particles/ml) indeed generates VNBs with 70 nm HA-AuNPs (Figure 8C) while VNBs are virtually absent with the 10 nm HA-AuNPs (Figure 8D), thus confirming the results in water.

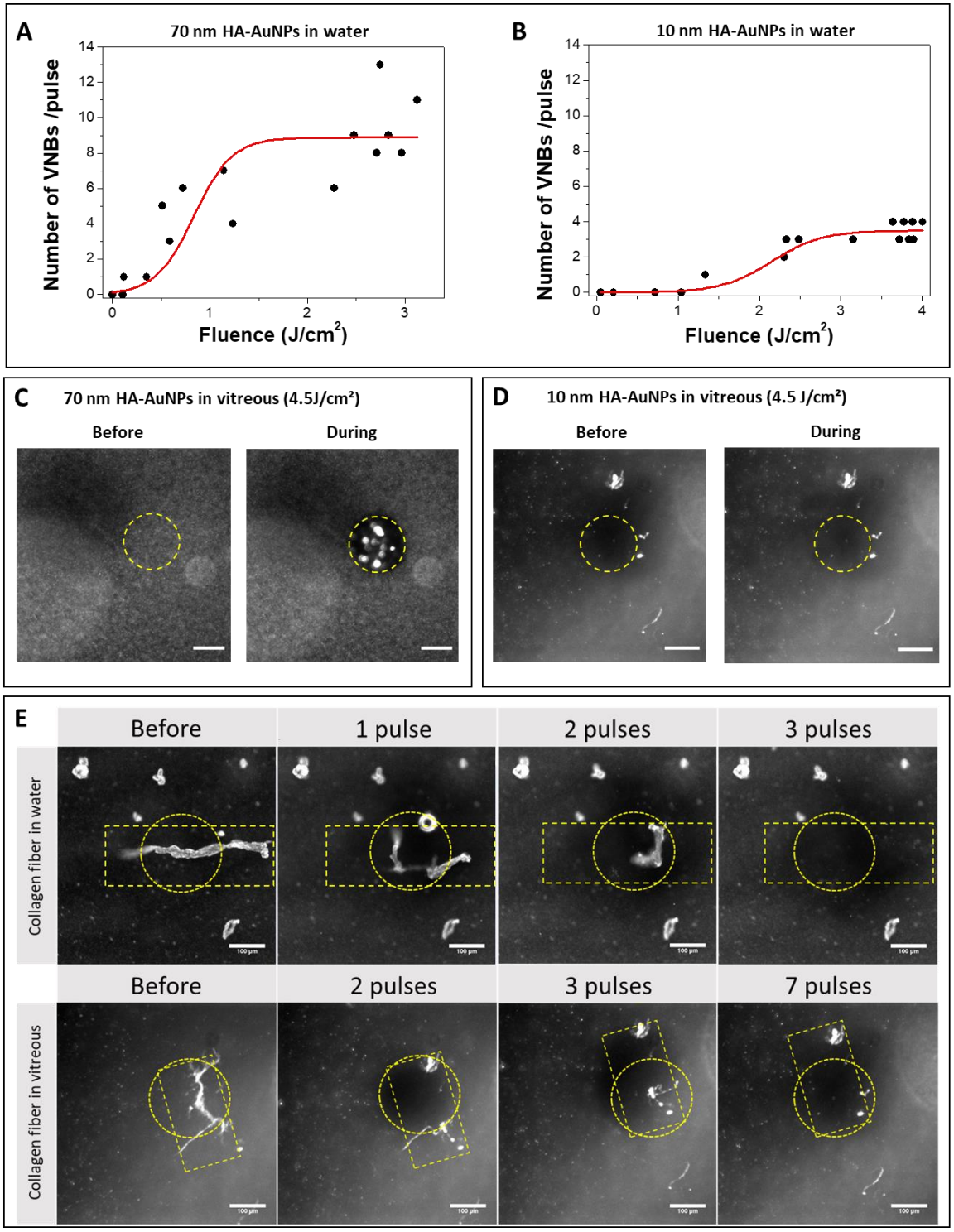

Figure 8. (A,B) The number of VNBs counted in the irradiated zone upon applying a single laser pulse to HA-AuNPs of a size of 70 nm (A) or 10 nm (B) in water. Note that a lower concentration of HA-AuNPs (10^{10} particles/ml) was used in Figure 8 A and B to be able to 'count' the number of VNBs. (C,D) Dark field images of bovine vitreous in which 70 nm (C) or 10 nm (D) HA-AuNPs are dispersed (10^{12} particles/ml), respectively before and during exposing a single laser pulse of 800 µJ (4.5 J/cm²). During the laser pulse VNBs (which reflect the laser light) can be observed as bright spots. (E) Representative dark field microscopy images of collagen fibers (in water and bovine vitreous (Movie S4)) carrying 10 nm HA-AuNPs respectively before and after applying one, or

several, 800 µJ laser pulses (4.5 J/cm²). The collagen concentration equaled 0.02 mg/ml while the concentration of the HA-AuNPs was 10^{12} particles/ml. For movies, see supplementary material.

However, while a single 800 µJ laser pulse (~4.5 J/cm²) did not generate VNBs from 10 nm HA-AuNPs 'freely' present in vitreous (Figure 8D), such a pulse was sufficient to destroy artificial collagen fibers (Figure 8E and Movie S4). This was made possible due to the outspoken accumulation (Figure 7B) and clustering (Figure 7C) of the 10 nm HA-AuNPs on the collagen fibers.

Photo-ablation of human vitreous opacities with 10 nm HA-AuNPs

Subsequently we investigated whether opacities present in vitreous of patients could be mechanically destroyed by vapor nanobubbles generated from locally accumulated 10 nm HA-AuNP. Because the composition, the size and shape of those opacities can vary from one patient to another, our strategy was tested on different patient samples (Figure 9). Interestingly, we found that, like on artificial collagen fibers (Figure 8E), human vitreous opacities of different size and shape could be destroyed using the same the concentration of 10 nm HA-AuNPs (10^{12} particles/ml) and the same intensity of the nanosecond laser pulses (800 µJ; ~4.5 J/cm²).

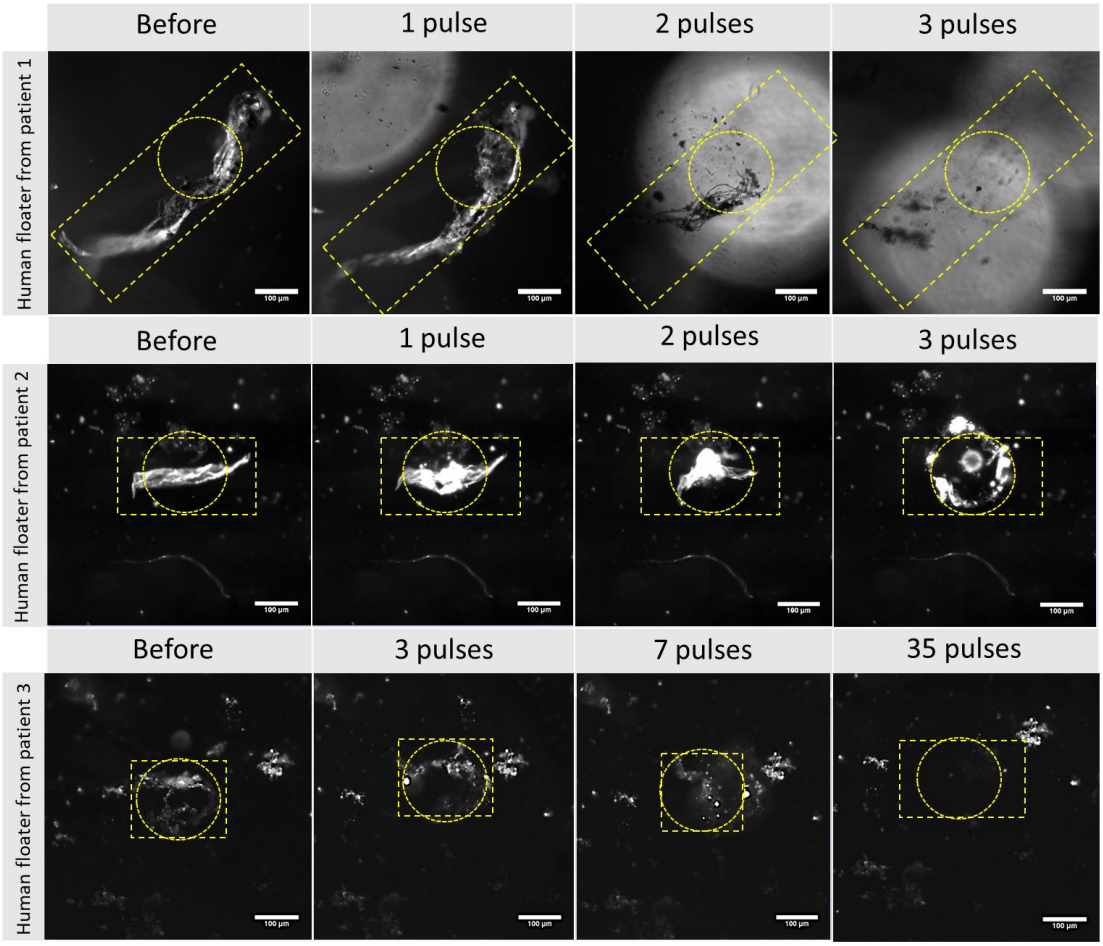

Figure 9**.** Dark field microscopy images of three human vitreous opacities (as obtained from three patients who underwent vitrectomy) carrying 10 nm HA-AuNPs, respectively before and after applying one, or several, laser pulses (800 µJ; ~4.5 J/cm²) (Movie S5). The concentration of the 10 nm HA-AuNPs suspension was 10^{12} particles/ml. The scale bar in (A) and (B) is 100 µm. The yellow dotted squares/rectangles indicate the position of the targeted fibers (A) or vitreous floaters (B). Dotted circles indicate the position of the laser beam. For movies, see supplementary material.

Human Müller cells survive the photo-ablation process

Clearly, a relevant question is to whether AuNPs, laser pulses and shock waves as generated from vapor nanobubbles may be harmful to the retina. To get some first insights on this, we performed toxicity studies on immortalized human Müller cells, the principal glial cell type in the retina with end feet inserted into the vitreo-retinal interface.[32] As Figure 10A indicates, when the cells are exposed to a single laser pulse of 200 µJ (~1.1 J/cm²) and 800 µJ (~4.5/cm²),

viability remained >80%. Also, when treated with 10 nm HA-AuNPs for 24h at a concentration which allows to break vitreous opacities (10^{12} particles/ml), cell viability remained >80% as for untreated cells (Figure 10B).

Subsequently we aimed to get an indication on the survival of Müller cells when nanobubbles are generated on collagen fibers representative of central vitreous opacities [16] and located a distance away from the cells. As Figure 10C shows, no effect was found on human Müller cells when the layer of collagen fibers (at a distance of 10 mm from the cells) was treated either with 200 µJ (~1.1 J/cm²) or 800 µJ (~4.5 J/cm²) laser pulses.

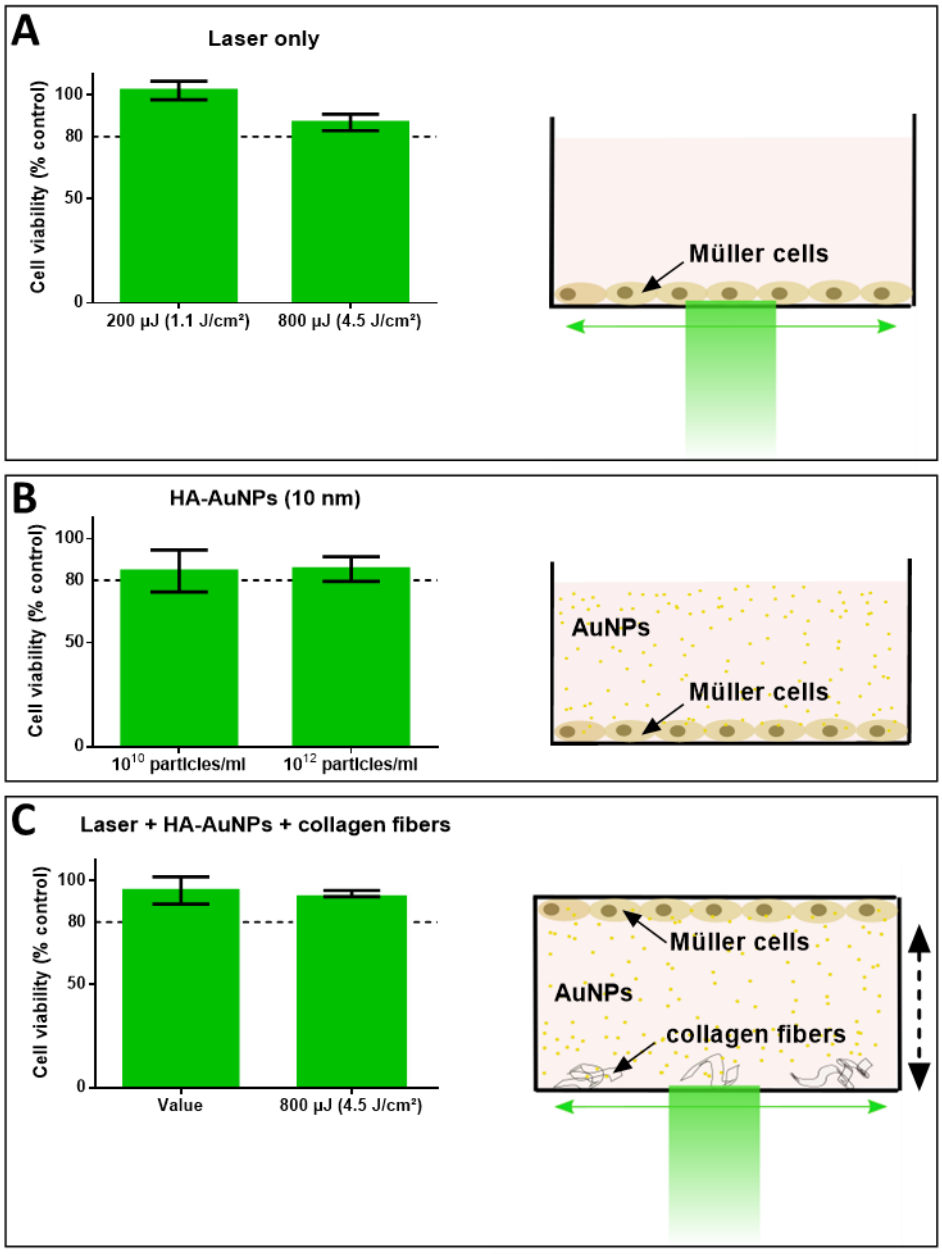

Figure 10. (A) Cell viability (MTT assay) of immortalized human Müller cells 24h after exposing the cells to the pulsed-laser only: each well was scanned (single scan) through the laser beam. (B) Cell viability 24h after treating the cells with 10 nm HA-AuNPs only (without applying laser light). (C) Cell viability of human Müller cells located at a distance of 10 mm from collagen fibers; the cells were first exposed to 10 nm HA-AuNPs (10^{12} particles/ml) for 24h; subsequently the layer of collagen fibers was scanned (single scan) through the laser beam. In the control experiments of A, B and C, cells were untreated.

Currently, the efficacy of YAG laser therapy for the treatment of vitreous opacities is far from optimal, lacking in objective quantitative evidence of efficacy. We propose to 'photo-ablate' vitreous opacities with a strategy allying pulsed-lasers and gold nanoparticles which might be promising for a more efficient and safer alternative to current treatments.

Clearly, the human vitreous is a complex, and not yet completely understood, biological matrix. Controlling the biophysical behavior of nanomaterials injected in such a complex matrix is highly challenging. After injection in bovine vitreous, we observed that cationic AuNPs are immobilized (Figure 5; Movie S2), in agreement with earlier observations with other types of cationic NPs.[25,26] Clearly, avoiding this represents a major challenge for AuNP assisted photo-ablation as immobilization of the gold nanoparticles at the injection site prevents them from reaching the vitreous opacities. Based on our previous work,[33] where we demonstrated that NP mobility in vitreous can be restored by applying a HA coating to the NPs, we observed that coating of AuNPs with HA avoids their immobilization in vitreous (Figure 5; Movie S3). Asakura *et al.* described that the collagen strands ('fibrils') in the biopolymer network of the vitreous are likely connected to HA (mediated by glycosaminoglycans (GAGs) such as chondroitin sulfates).[34] The negatively charged HA on the collagen strands keep the strands sufficiently apart. This minimizes light scattering, keeping the vitreous transparent. This hypothesis was further confirmed later by Scott [35] who describes a three-component complex (collagen-GAG-HA-GAG-collagen) forming the vitreous network with possible interactions occuring between HA and GAG.[36] As schematically presented in Figure 11A, electrostatic

repulsions may therefore possibly occur between HA-AuNPs and HA connected to the collagen strands, explaining why HA-AuNPs remain mobile in vitreous. Instead, cat-AuNPs likely bind to the negatively charged HA molecules, causing immobilization to the collagen strands (Figures 3 and 5 and Movie S2).

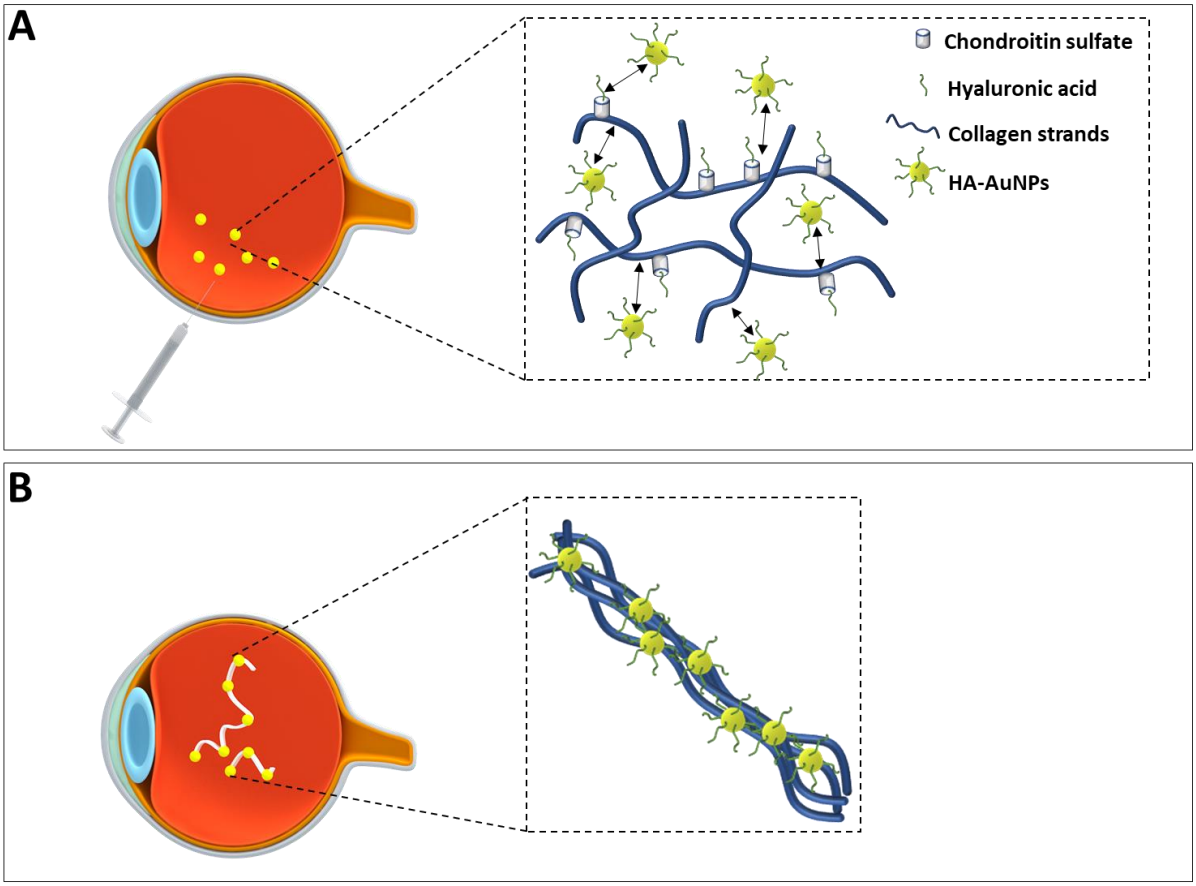

Figure 11. (A) Schematic representation of the fate of HA-coated AuNPs in the vitreous. (B) Schematic representation of the binding of HA-AuNPs to a vitreous opacity.

Surprisingly, while the negatively charged HA-AuNPs do not seem to interact with the collagen strands of the biopolymer network in vitreous (Figure 5 and Movie S3; and as schematically shown in Figure 11A), we found that they do bind to type I collagen fibers (Figure 6) and human vitreous opacities (Figure 9), similar to what was observed for cat-AuNPs (Figure 2). A possible explanation is the presence of both anionic sites and cationic groups on the surface of the collagen fibers that comprise vitreous opacities, as suggested in earlier studies.[37,38] Also, as vitreous opacities are often present in liquefied parts of the vitreous, one can assume that HA

is absent on the surface of the opacities or, at least, present in a lower concentration in their immediate surroundings, as previously suggested by Sebag and Balazs.[39] This absence of HA (and thus absence of electrostatic interactions) might explain why HA-AuNPs keep their binding capacity to opacities, as schematically illustrated in Figure 11B.

We investigated the potential of 10 nm AuNPs for the photo-ablation process as smaller particles diffuse more easily through vitreous (a requirement to reach the floaters)[23] while they scatter less light which might provide more comfort to the patient. At laser fluences used in our study, when freely dispersed in water or vitreous 10 nm sized HA-AuNPs seemed too small to generate VNBs (Figure 8), this in opposite to the 70 nm sized HA-AuNPs; this size dependency was indeed expected and in agreement with previous reports.[41,51,52] Importantly, however, we noticed that 10 nm HA-AuNPs bind and cluster on the surface of collagen fibers (Figure 7). This binding and clustering of the AuNPs on the fibers improves light absorption and lowers the laser energy required to generate nanobubbles. This is an interesting finding as it allows to use laser pulses which are strong enough to generate nanobubbles on the fibers while they are too weak to generate nanobubbles in the surroundings. This 'fiber-specific nanobubble generation' is attractive as it may minimize potential damage to the surrounding vitreous and tissues.

Since human vitreous opacities might contain several types of collagen and since the morphology and structure of floaters is highly variable between patients as well, we evaluated the photo-ablation potential of 10 nm HA-AuNPs on vitreous opacities obtained during vitrectomy on patients with vision degrading myodesopsia. Figure 9 and Movie S5 show representative examples. We observed that all opacities in the various human vitreous samples we investigated could be broken using experimental settings similar to the ones which allow to break type I collagen fibers (Figure 8E). We also observed that the morphology of floaters varied from one patient to another. Indeed, while some floaters give the impression of membranes, others seemed smaller and denser. The structural heterogeneity of floaters also

implies that for some of them more laser pulses were needed for destruction, as observed in Figure 9 for floaters obtained from patient 3.

In traditional YAG laser vitreolysis, floaters are destroyed by plasma formation [42] requiring laser pulses at very high energy densities up to 5000 J/cm². Since a single YAG laser pulse typically has an energy in the order of 10 mJ,[10] it means that the laser beam needs to be tightly focused to less than 20 µm diameter onto the floaters to achieve local photo destruction. Considering that vitreous opacities can have much larger dimensions, up to 1000 shots may be needed to destroy a single opacity, amounting to a total light dose of 10^4 mJ. In our approach, however, we use AuNPs as sensitizing agent to enhance light absorption so that much lower energy densities and total light doses are needed to achieve the same effect. Indeed, in this study the laser beam was 150 µm (diameter) and pulses had an energy of 0.8 mJ. This means that the light energy density was as low as 4.5 J/cm², which is approximately 1000 times less than what is used for YAG laser therapy. In addition, since consequently the laser beam can be much larger, fewer laser pulses are needed to completely destroy the fibers. Indeed, we needed about 10 pulses to destroy opacities, which corresponds to a total light dose of about 10 mJ, again approximately 1000 times less than YAG laser therapy. Taken together, gold nanoparticle assisted photo-ablation of vitreous opacities might be less damaging for the posterior segment of the eye as a significantly lower number of weaker laser pulses seem to be sufficient to break opacities. Another practical advantage of being able to use a larger laser beam is that the distance along the optical axis (*i.e.* the direction of light propagation) over which a suitable energy density is achieved for photo-ablation is much larger. Indeed, assuming a Gaussian beam profile for simplicity, the depth of focus scales with the square of the beam spot size. This means that for our laser beam of 150 µm diameter, the depth of focus is at least 56 times ((150 µm /20 µm)²) more extended as compared to the < 20 µm beam for the YAG laser. Practically this means that 3D focusing onto the floater is not such a stringent requirement, making the whole procedure much easier to perform.

These advantages come, of course, at the expense of having to introduce sensitizing AuNPs into the vitreous, which raises questions about potential toxic effects. Even though the toxicity of several types of nanoparticles to the retina has been reported in literature,[43] few reports study toxicological effects of AuNPs on the retina. It has been reported that 20 nm AuNPs intravenously injected in rabbits were able to cross the blood retinal barrier without affecting cell viability or inducing structural changes in the retina.[44] In another study AuNPs were intravitreally injected in rabbits and histological observations were performed up to one month without showing clear signs of toxicity.[45] Furthermore, it is also known that AuNPs have anti-angiogenic and anti-inflammatory properties which can improve the treatment of ophthalmological diseases.[46] This relative safety of using AuNPs was also confirmed in our preliminary toxicity study on Müller cells, which possess end feet at the vitreo-retinal interface. Indeed, when incubated with 10^{12} NP/ml, cell viability remained > 80% which is often regarded as the acceptable toxicity limit for in-vitro cell experiments. This was a worst-case experiment as *in vivo* the effective dose which reaches the cells will be limited due to dilution effects. Another concern may be if cells are affected by the laser light itself. Even though our approach uses light intensities and total doses that are much less than what is currently used in traditional YAG laser therapy, we double checked this explicitly on Müller cells *in vitro*. As expected, cell viability remained very good. Finally, we tested if the generation of VNBs from vitreous opacities located at the centre of the vitreous body may be harmful to nearby retinal cells. We noticed that, in case collagen fibers are located at a distance of 10 mm from the Müller cells (taken as a representative position of vitreous opacities from the retina), no toxicity was observed (Figure 10C).

Regarding the further translation of gold nanoparticle assisted photo-ablation into clinical practice, also the half-life of the gold particles in the vitreous is of major importance. Indeed, the gold nanoparticles should stay for a sufficiently long time in the vitreous to allow the photo-ablation of opacities. Measuring the half-life of gold nanoparticles in animal models could make sense. However, to which extent this information would be sufficiently predictive for the

clearance of gold nanoparticles in human eyes is not so clear. Following the mechanistic model described by Hutton-smith *et al.*,[47] the half-life of intravitreally-injected drugs/nanoparticles can be (partially) estimated from their diffusion coefficient in vitreous. For gold nanoparticles of 10 nm, taking into account their diffusion coefficient in vitreous and the volume of vitreous in human eyes, we estimate the half-life in vitreous to be approximately one day. It suggests that the intravitreal injection of the gold nanoparticles and the laser treatment should be performed at the same day.

Conclusions

In this study, we have presented a nanomaterial-based approach which might be promising for the treatment of vitreous opacities that cause vision degrading myodesopsia. We conclude that vapor nanobubbles, which arise upon applying nanosecond laser pulses to gold nanoparticles, deliver sufficient mechanical energy to break human opacities as present in the vitreous of patients who underwent vitrectomy. We observed that gold particles coated with hyaluronic acid, being a major component of vitreous, do not get stuck in vitreous while they accumulate on the opacities. This clustering of gold nanoparticles lowers the intensity of the laser pulses needed to generate vapor nanobubbles on the opacity. Local 'floater-specific nanobubble generation' is attractive as it might preserve the surrounding vitreous and ocular tissues. Due to the clustering of the gold particles on the opacities, even small (10 nm) gold particles generate vapor nanobubbles on the opacities which can break them. Such small nanoparticles are especially attractive as we showed that they easily diffuse in vitreous, a requirement to reach the opacities after intravitreal injection, while they scatter less light which might provide more comfort to the patient. Important as well, compared to current YAG laser therapy for floaters in which patients receive hundreds of mJoule-shots in the eye, a much smaller number of low intensity laser shots (µJoule) seem sufficient to break vitreous opacities causing floaters. In

conclusion, our experiments have shown promising results to treat vitreous disorders which may enlarge the therapeutic perspectives on the use of pulsed-lasers and nanotechnology in the posterior segment of the eye, being promising medical technologies as recently highlighted by Palanker.[48]

Methods/Experimental

Materials

The following materials were used as obtained: $HAuCl_4$ (Aldrich); sodium citrate (Aldrich); sodium L-ascorbate (Sigma-Aldrich); hyaluronic acid 20 kDa (HA) (Aldrich); poly(diallyl-dimethyl-ammonium chloride) (PDDAC) solution (20 wt. % in H_2O; Aldrich), rat tail collagen type I acid solution (Sigma-Aldrich) and Col-F (Immunochemistry Technologies LLC).

Synthesis of gold nanoparticles

The synthesis of 70-80 nm AuNPs was performed using the Turkevich method.[49] Therefore, to 150 mL of a 0.2 mM chloroauric acid ($HAuCl_4$) solution (in water), 0.5 mL of a 0.01 M citrate solution (in water; as reducing agent; corresponding to a 1:1 Au/citrate molar ratio) was added. To obtain 'gold seeds' this mixture was heated (to boiling temperature) and rapidly stirred for 30 min. The gold seeds were overgrown by addition of 0.005 M gold ion (Au^{3+} in water) and, subsequently, added with an ascorbate solution (0.005 M in water; as a strong reducing agent) until the UV-vis extinction spectrum (as measured by a Nanodrop 2000c spectrophotometer) of 70-80 nm AuNPs was observed *i.e.* extinction between 538-542 nm.

The synthesis of 10 nm AuNPs was performed using ascorbate as reducing agent. A typical synthesis consists in mixing $HAuCl_4$ (in water) and sodium ascorbate (in water) at equimolar ratios (concentration 0.2 mM, final volume 100 mL) under rapid stirring. We allowed the reaction to proceed until the UV-vis extinction spectrum of 10 nm AuNPs was observed.

Measuring the size and concentration of the gold nanoparticles

The AuNPs were characterized by UV-vis spectroscopy, dynamic light scattering (DLS), TEM and electrodynamic modeling using Mie theory. The concentration of the AuNPs in the

dispersions was estimated from the extinction of the dispersions as measured at the maximal extinction wavelength (Ext), as follows (equation 1):[50]

$$[AuNPs]\left(\frac{number}{ml}\right) = Ext/(b \times \sigma\mathrm{EXT})$$

Where 'b' is the optical path (1 cm) and 'σ_{EXT}' (cm^2) is the theoretical extinction cross section for spherical particles obtained by Mie theory calculations.[51]

Surface coating of the gold nanoparticles

The Au nanoparticles were coated with respectively negatively charged HA (HA-AuNPs) or positively charged PDDAC (cat-AuNPs). Typically, coating with HA was performed by adding 3 mg HA (previously dissolved in 1 mL distilled deionized (ddi) water) to 50 mL of an AuNP dispersion in water (2-4 pM). Coating with PDDAC was performed by addition of 11.9 mg of PDDAC (previously dissolved in 1 mL ddi water) to 50 mL of a dispersion of HA-coated AuNPs (2-4 pM). After reaction overnight, thus obtained coated gold nanoparticles were washed by centrifugation (10 min at 13000g for 10 nm AuNPs and 5 min at 2000g for 70-80 nm AuNPs) and resuspended in water. To confirm a successful coating of the gold nanoparticles, DLS and zeta potential measurements were performed (Zetasizer Nano, Malvern).

Simulation of the optical properties of gold nanoparticles

The optical responses (*i.e.* scattering, absorption and extinction) of AuNPs were computed using Mie theory, which constitutes an exact solution to the problem of absorption and scattering of light by an object composed by concentric spheres.[52] In particular, we used the Generalized Multiparticle Mie Theory (GMM) formulation developed by Xu.[53] This method is able to exactly solve the complex problem of interaction between an electromagnetic field and an aggregate of spheres, and was used to simulate the extinction, scattering and absorption cross sections. In all the calculations presented in this work the dielectric function tabulated by Palik for Au was employed.[54] In the calculations performed in this work the NPs were excited by a

plane wave with an incidence pointing vector (propagation direction) normal to the surface. As the GMM code is restricted to applications in homogeneous media, we used an effective medium approximation [55] to account for the interface between the particle surface and the aqueous environment. We considered that particles were immersed in a dielectric environment with an effective refractive index (n_{eff}) of 1.35, which was calculated as the weighted average of 20% of the refractive index of collagen (n_r 1.41) and 80 % of the refractive index of water (n_r 1.33).[56]

Formation of collagen fibers as a model for vitreous opacities

Collagen I from rat tail was dissolved in PBS (0.2 mg/ml); the pH of the collagen solution was increased to 7.4 with NaOH (0.1N). Subsequently, the collagen solution was incubated at 37°C for one hour. To follow the fibrillation process, turbidity experiments were performed by measuring the absorbance of the collagen suspension (λ400 nm) at 37°C (using a NanoDrop 2000c spectrophotometer). Collagen fibers were stained with Col-F probe.[22] Therefore, the collagen fiber dispersion was incubated for 4h at room temperature with Col-F (in DMSO) to reach a final Col-F concentration of 20 µM and subsequently centrifuged to remove the excess of the probe.

Vitreous samples

Bovine vitreous containing collagen type I fibers

Bovine eyes were enucleated less than one hour after cows were slaughtered (slaughterhouse Zele, Belgium). Since vitreous has a very fragile structure, it was carefully removed from the globe. First, 200 to 400 µl was carefully cut and placed on a glass-bottomed culture dish. Subsequently 50 µl of the suspension of collagen type I fibers was injected in the vitreous sample using a 1 ml syringe equipped with a 21.5G needle and let to equilibrate at room temperature for 30 min. AuNPs were then randomly injected in the sample (no more than 40 µl per injection) using a 1 ml syringe equipped with a 30G needle (no more than 5 injection spots

per vitreous sample to avoid extensive liquefaction). The sample was let to equilibrate for 30 min prior to applying (nanosecond) laser pulses (Opolette HE 355 LD laser, OPOTEK Inc.)

Human vitreous containing opacities

Samples of vitreous containing opacities were collected at the VMR Institute for Vitreous Macula Retina (Huntington beach, CA, USA) from patients undergoing vitrectomy for the treatment of Vision Degrading Myodesopsia.[7,57,58] The study protocol adhered to the Declaration of Helsinki. Prior to surgery, patients gave a written informed consent that has been reviewed and accepted by the ethical committee of Saint Joseph Health Center for clinical research (Irvine, CA, USA). After vitrectomy the (undiluted) samples were frozen and stored at -80°C until further use. After thawing the human vitreous samples, they were directly mixed with an equal volume of a dispersion of AuNPs (typically 10^{12} NPs/ml in water). The samples were then allowed to equilibrate for 30 min at room temperature prior to applying (nanosecond) laser pulses.

Measuring the mobility of AuNPs in vitreous through SRAF

SRAF (scattering recovery after fragmentation) measurements were performed to determine the mobility (diffusion) of the AuNPs in the bovine vitreous. Following our experience on fluorescence recovery after photobleaching (FRAP),[59,60] we here propose SRAF and used it to determine the diffusion of light scattering AuNPs. FRAP is a well-known fluorescence microscopy-based technique that is commonly used in pharmaceutical and biological research to assess the diffusion of fluorescent molecules or nanoparticles in various media [61] and, as we showed more recently, to measure the size of fluorescent (nano)particles dispersed in complex biofluids like serum.[62] As Figure 12 (top panel, first row) illustrates, FRAP is performed by applying a high intensity laser beam in a defined region of (typically) a few micrometers in size (’bleached’ region) which leads to the destruction of the fluorophores present in this area. In case the fluorescent molecules are mobile a recovery of fluorescence in the bleached region will subsequently occur over time. From this fluorescence recovery curve the diffusion coefficient

of the fluorescent molecules can be calculated.[61] Inspired by the FRAP method we measured the mobility of the light scattering (non-fluorescent) gold nanoparticles using dark field microscopy. Therefore, as Figure 12 (top panel, second row) illustrates, first the intensity of the scattered light (originating from the gold NPs) in a micrometer sized zone in the sample was measured. Second, a single laser pulse was applied in that zone. As we know from the literature and our previous observations that this 'fragments' the gold NPs,[63] and therefore decreases their size, light scattering in this 'fragmentation zone' decreases, resulting in a local dark spot in the images. From the light scattering recovery in the fragmentation zone, due to the diffusion of unaffected AuNPs from the surroundings in the fragmentation zone, the mobility (diffusion coefficient) of the gold nanoparticles could be quantified.

For SRAF mobility experiments in water, 5 µL of AuNPs suspension (10^{12} particles/ml in water) was placed on a microscopy slide. For measuring the mobility of the AuNPs in the vitreous through SRAF, 40 µL of a highly concentrated suspension of AuNPs (typically 10^{12} particles/ml in water) was injected in a bovine vitreous sample (200-400 µl) contained in a glass-bottomed dish and allowed to equilibrate for 30 min. Then samples were placed under the dark field microscope (10x objective) and illuminated with the nanosecond laser (Opolette HE 355 LD, OPOTEK Inc; 561 nm; 200 µJ; 1.1 J/cm²; 1 pulse) to fragment the AuNPs; subsequently the increased intensity of scattered light in the fragmentation zone was recorded for about 10 min. Recovery curves were obtained from NIS software. As the nanosecond pulsed-laser beam was fairly circular and uniform, the diffusion coefficient (D; in µm²/s) was estimated according to $D = w^2/4\tau$ (equation 2) with w the radius (µm) of the fragmentation zone and τ the half-life of scattering recovery (s).[64] The curves were fitted using a third order polynomial function. Note that in all SRAF experiments 70 nm AuNPs were used since they scatter the light sufficiently.

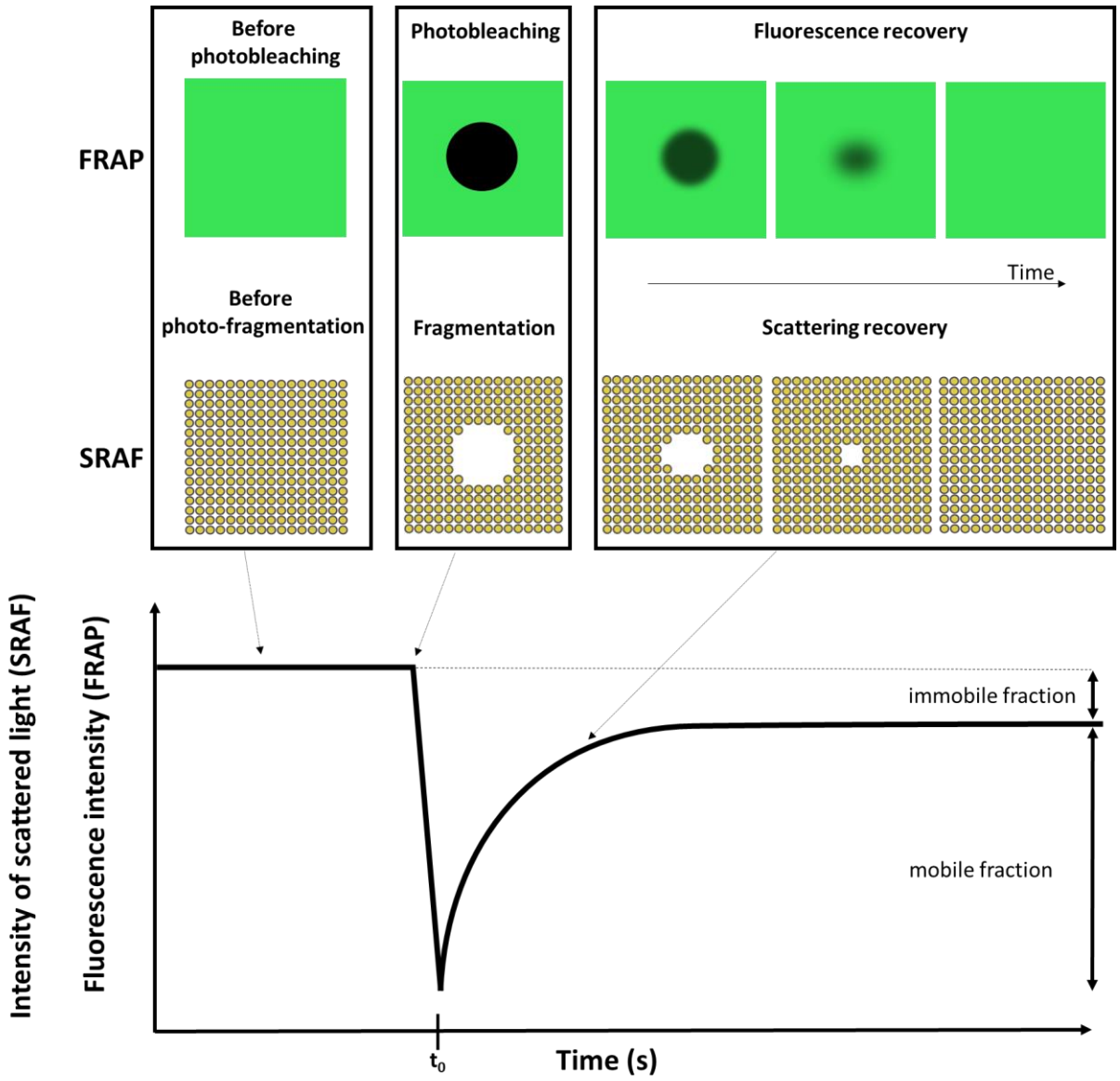

Figure 12. Scattering recovery after fragmentation (SRAF) and its analogy with fluorescence recovery after photobleaching (FRAP).

Nanoparticle tracking analysis (NTA)

To measure the diffusion of the AuNPs in water, NTA measurements were performed with a Nanosight instrument (Malvern). Therefore, AuNPs were diluted in water (10^{10} NPs/ml) and injected with a sterile syringe in the sample chamber. Measurements were made using the scattering mode. All measurements were performed at room temperature.

Photo-ablation of collagen fibers and human vitreous opacities

Photo-ablation experiments were performed on the samples described in the previous sections (collagen fibers in bovine vitreous and human vitreous containing opacities). First, dark field microscopy imaging was performed to locate and align the nanosecond laser on the collagen fibers or human vitreous opacities in the sample. To generate vapor nanobubbles, 7ns laser pulses were used. The wavelength of the laser light was 561 nm which corresponds to the plasmon peak of 70-80 nm AuNPs. A beam expander (#GBE05-A, Thorlabs) combined with iris diaphragm (#D37SZ, Thorlabs) was used to adjust the diameter of the laser beam to 150 µm. The laser pulse energy was monitored by an energy meter (J-25MB-HE&LE, Energy Max-USB/RS sensors, Coherent) synchronized with the pulsed-laser. The length of the collagen fibers was determined from the microscopy images using ImageJ software.

Transmission electron microscopy to study the binding of AuNPs to collagen fibers

Transmission electron microscopy (TEM) images were obtained using a JEM-JEOL 1120 EXII under an accelerating voltage of 80 kV. One drop (~ 50 µL) of sample was added onto a holey carbon-formvar coated copper TEM grid (100 mesh).

Counting the number of VNBs generated per laser pulse

The number of VNBs generated per laser pulse was determined by dark-field microscopy as we described before.[65] Dispersions of HA-AuNPs in water (10^{10} NPs/mL) were applied in a 50 mm glass bottom dish (MatTek Corporation, US). After an equilibration of 1 hour, a single 7 ns laser pulse was applied and the number of VNBs were counted in the irradiated area (~150 µm laser beam diameter) of the dark field images. Dark field images were recorded with an illumination time of 10 ms after firing the laser pulse so as to capture the short-lived VNBs. As the laser fluence (*i.e.* the energy density calculated as the energy of a single laser pulse divided by the laser beam area), increases, more AuNPs in the irradiated zone will form VNBs. Graphs, which show the number of VNBs as function of the laser fluence, were plotted.

Cell culture and toxicity studies

Human Müller cells (MIO-M1) (ATCC®) were cultured in high glucose Dulbecco's modified Eagle's medium GlutaMAX™, supplemented with 10% fetal bovine serum, 2 mM L-Glutamine and 100 U/mL penicillin-streptomycin (InVitrogen). Cells were regularly tested for *Mycoplasma* with the Mycoalert™ detection kit (Lonza, Rockland, ME) according to the manufacturer's instruction. Cells were grown in 96-well plate for 24h (7000 cells/well) at 37°C and under 5% CO_2 to 80-90% confluence. Cells were passaged using DPBS (Gibco-Invitrogen) and trypsin-EDTA (0.25%, Gibco-Invitrogen).

To test the impact of the laser pulses on cell viability, the cells growing in wells were scanned through the laser beam (single scan; 200 µJ (~1.1 J/cm²) or 800 µJ (~ 4.5 J/cm²); 20 Hz frequency) using an electronic microscopy stage (HLD117, Prior Scientific, USA). The scanning speed was 2.1 mm/s and the distance between subsequent lines was 0.1 mm. With these parameters, one can assume that each cell was exposed to one single laser pulse.[66] Cell viability was measured by MTT assay (Sigma-Aldrich) 24 hours after laser treatment. In each well, the cell medium was removed and replaced by the MTT reagent (100 µl, 1.5 mM) which was incubated with the cells for 3 hours at 37 °C. Afterwards, in each well, the reagent was replaced by DMSO to dissolve the formazan crystals, and the plate was placed on a shaker for 1 hour. The readout was performed using a plate spectrophotometer (PerkinElmer VICTOR^3 1420 Multilabel Counter®) measuring the absorbance at 595 nm and 650 nm as a reference wavelength.

To test the impact of the laser pulses in the presence of gold NPs on cell viability, cells were grown in a 96-well plate for 24 hours (7000 cells/well). The cell medium was then discarded and replaced by fresh cell medium containing 10 nm HA-AuNPs (10^{12} particles/ml) and collagen fibers (0.02 mg/ml). Cells were incubated for 4 hours. Subsequently, a microscope cover glass was placed on the top of the wells and stuck with nunc sealing tapes. This allowed to invert the cell plate without leakages. By inverting the cell plate (as illustrated in panel C of

Figure 10), the laser beam first hit the collagen fibers while the cell monolayer is located at approximately 10 mm (corresponding to the height of a well), a situation which corresponds to an opacity located at the center of the vitreous.[16] Each well was then scanned through the laser beam as described above. Immediately after, cell viability was measured by MTT assay as described above.

Statistical significance

Student's t-test (two-tailed) was used to calculate statistical significance. Differences were considered significant when $p < 0.05$.

Supporting information

Movie S1. Diffusion measurements (SRAF) on HA-AuNPs in water.

Movie S2. Diffusion measurements (SRAF) on cat-AuNPs in bovine vitreous.

Movie S3**.** Diffusion measurements (SRAF) on HA-AuNPs in bovine vitreous.

Movie S4. HA-AuNP assisted photo-ablation of collagen fibers in bovine vitreous.

Movie S5. HA-AuNP assisted photo-ablation of a human vitreous opacity.

Acknowledgments

Authors would like to thank Victor Jardel for the illustrations and FWO, ERC and BOF-UGent for financial support.

References

(1) Rambaran, R. N.; Serpell, L. C. Amyloid Fibrils. *Prion* **2008**, *2*, 112–117.
(2) Sebag, J. Age-Related Changes in Human Vitreous Structure. *Graefes Arch. Clin. Exp. Ophthalmol.* **1987**, *225*, 89–93.
(3) Wagle, A. M.; Lim, W.-Y.; Yap, T.-P.; Neelam, K.; Au Eong, K.-G. Utility Values Associated with Vitreous Floaters. *Am. J. Ophthalmol.* **2011**, *152*, 60-65.e1.
(4) Sebag, J. Floaters and the Quality of Life. *Am. J. Ophthalmol.* **2011**, *152*, 3-4.e1.
(5) Wa, C.; Sebag, J. Safety of Vitrectomy for Floaters. *Am. J. Ophthalmol.* **2011**, *152*, 1077; author reply 1077-1078.
(6) J, S.; Km, Y.; Ca, W.; Lc, H.; Aa, S. Vitrectomy for Floaters: Prospective Efficacy Analyses and Retrospective Safety Profile. *Retina Phila. Pa* **2014**, *34*, 1062–1068.
(7) Sebag, J.; Yee, K. M. P.; Nguyen, J. H.; Nguyen-Cuu, J. Long-Term Safety and Efficacy of Limited Vitrectomy for Vision Degrading Vitreopathy Resulting from Vitreous Floaters. *Ophthalmol. Retina* **2018**, *2*, 881–887.
(8) Milston, R.; Madigan, M. C.; Sebag, J. Vitreous Floaters: Etiology, Diagnostics, and Management. *Surv. Ophthalmol.* **2016**, *61*, 211–227.
(9) Abdelkawi, S. A.; Abdel-Salam, A. M.; Ghoniem, D. F.; Ghaly, S. K. Vitreous Humor Rheology After Nd:YAG Laser Photo Disruption. *Cell Biochem. Biophys.* **2014**, *68*, 267–274.
(10) Procedure Guide: Vitreous Opacities - Ellex https://www.ellex.com/resources/procedure-guide-vitreous-opacities/ (accessed Nov 14, 2018).
(11) Delaney, Y. M.; Oyinloye, A.; Benjamin, L. Nd:YAG Vitreolysis and Pars Plana Vitrectomy: Surgical Treatment for Vitreous Floaters. *Eye* **2002**, *16*, 21–26.
(12) Shah, C. P.; Heier, J. S. YAG Laser Vitreolysis vs Sham YAG Vitreolysis for Symptomatic Vitreous Floaters: A Randomized Clinical Trial. *JAMA Ophthalmol.* **2017**, *135*, 918–923.
(13) Koo, E. H.; Haddock, L. J.; Bhardwaj, N.; Fortun, J. A. Cataracts Induced by Neodymium–Yttrium-Aluminium-Garnet Laser Lysis of Vitreous Floaters. *Br. J. Ophthalmol.* **2017**, *101*, 709–711.
(14) Cowan, L. A.; Khine, K. T.; Chopra, V.; Fazio, D. T.; Francis, B. A. Refractory Open-Angle Glaucoma After Neodymium–Yttrium-Aluminum-Garnet Laser Lysis of Vitreous Floaters. *Am. J. Ophthalmol.* **2015**, *159*, 138–143.
(15) Huang, K.-H.; Weng, T.-H.; Chen, Y.-J.; Chang, Y.-H. Iatrogenic Posterior Lens Capsule Rupture and Subsequent Complications Due to Nd:YAG Laser Vitreolysis for Vitreous Floaters: A Case Report. *Ophthalmic Surg. Lasers Imaging Retina* **2018**, *49*, e214–e217.
(16) Tsai, W. F.; Chen, Y. C.; Su, C. Y. Treatment of Vitreous Floaters with Neodymium YAG Laser. *Br. J. Ophthalmol.* **1993**, *77*, 485–488.
(17) Vandorselaer, T.; Van De Velde, F.; Tassignon, M. J. Eligibility Criteria for Nd-YAG Laser Treatment of Highly Symptomatic Vitreous Floaters. *Bull. Soc. Belge Ophtalmol.* **2001**, 15–19.
(18) Qin, Z.; C. Bischof, J. Thermophysical and Biological Responses of Gold Nanoparticle Laser Heating. *Chem. Soc. Rev.* **2012**, *41*, 1191–1217.
(19) Ghosh, S. K.; Pal, T. Interparticle Coupling Effect on the Surface Plasmon Resonance of Gold Nanoparticles: From Theory to Applications. *Chem. Rev.* **2007**, *107*, 4797–4862.
(20) Lukianova-Hleb, E. Y.; Mutonga, M. B. G.; Lapotko, D. O. Cell-Specific Multifunctional Processing of Heterogeneous Cell Systems in a Single Laser Pulse Treatment. *ACS Nano* **2012**, *6*, 10973–10981.
(21) Sebag, J. *Vitreous: In Health and Disease*; Springer, 2014.

(22) Biela, E.; Galas, J.; Lee, B.; Johnson, G. L.; Darzynkiewicz, Z.; Dobrucki, J. W. Col-F, a Fluorescent Probe for Ex Vivo Confocal Imaging of Collagen and Elastin in Animal Tissues. *Cytom. Part J. Int. Soc. Anal. Cytol.* **2013**, *83*, 533–539.
(23) Xu, Q.; Boylan, N. J.; Suk, J. S.; Wang, Y.-Y.; Nance, E.; Yang, J.-C.; McDonnell, P.; Cone, R.; Duh, E. J.; Hanes, J. Nanoparticle Diffusion in, and Microrheology of, the Bovine Vitreous Ex Vivo. *J. Control. Release Off. J. Control. Release Soc.* **2013**, *167*, 76–84.
(24) Käsdorf, B. T.; Arends, F.; Lieleg, O. Diffusion Regulation in the Vitreous Humor. *Biophys. J.* **2015**, *109*, 2171–2181.
(25) Martens, T. F.; Vercauteren, D.; Forier, K.; Deschout, H.; Remaut, K.; Paesen, R.; Ameloot, M.; Engbersen, J. F.; Demeester, J.; De Smedt, S. C.; Braeckmans, K. Measuring the Intravitreal Mobility of Nanomedicines with Single-Particle Tracking Microscopy. *Nanomed.* **2013**, *8*, 1955–1968.
(26) Peeters, L.; Sanders, N. N.; Braeckmans, K.; Boussery, K.; Voorde, J. V. de; Smedt, S. C. D.; Demeester, J. Vitreous: A Barrier to Nonviral Ocular Gene Therapy. *Invest. Ophthalmol. Vis. Sci.* **2005**, *46*, 3553–3561.
(27) Martens, T. F.; Peynshaert, K.; Nascimento, T. L.; Fattal, E.; Karlstetter, M.; Langmann, T.; Picaud, S.; Demeester, J.; De Smedt, S. C.; Remaut, K.; Braeckmans, K. Effect of Hyaluronic Acid-Binding to Lipoplexes on Intravitreal Drug Delivery for Retinal Gene Therapy. *Eur. J. Pharm. Sci.* **2017**, *103*, 27–35.
(28) Lombard, J.; Biben, T.; Merabia, S. Threshold for Vapor Nanobubble Generation Around Plasmonic Nanoparticles. *J. Phys. Chem. C* **2017**, *121*, 15402–15415.
(29) Lapotko, D. Optical Excitation and Detection of Vapor Bubbles around Plasmonic Nanoparticles. *Opt. Express* **2009**, *17*, 2538–2556.
(30) Lapotko, D. O.; Lukianova-Hleb, E. Y.; Oraevsky, A. A. Clusterization of Nanoparticles during Their Interaction with Living Cells. *Nanomed.* **2007**, *2*, 241–253.
(31) Fraire, J. C.; Pérez, L. A.; Coronado, E. A. Cluster Size Effects in the Surface-Enhanced Raman Scattering Response of Ag and Au Nanoparticle Aggregates: Experimental and Theoretical Insight. *J. Phys. Chem. C* **2013**, *117*, 23090–23107.
(32) Sebag, J. Age-Related Differences in the Human Vitreoretinal Interface. *Arch. Ophthalmol. Chic. Ill 1960* **1991**, *109*, 966–971.
(33) Martens, T. F.; Remaut, K.; Deschout, H.; Engbersen, J. F. J.; Hennink, W. E.; van Steenbergen, M. J.; Demeester, J.; De Smedt, S. C.; Braeckmans, K. Coating Nanocarriers with Hyaluronic Acid Facilitates Intravitreal Drug Delivery for Retinal Gene Therapy. *J. Controlled Release* **2015**, *202*, 83–92.
(34) Asakura, A. [Histochemistry of Hyaluronic Acid of the Bovine Vitreous Body by Electronmicroscopy]. *Nippon Ganka Gakkai Zasshi* **1985**, *89*, 179–191.
(35) Scott, J. E. The Chemical Morphology of the Vitreous. *Eye Lond. Engl.* **1992**, *6 (Pt 6)*, 553–555.
(36) Scott, J. E. Supramolecular Organization of Extracellular Matrix Glycosaminoglycans, *in Vitro* and in the Tissues. *FASEB J.* **1992**, *6*, 2639–2645.
(37) Tang, R.; Liao, X.-P.; Shi, B. Heterogeneous Gold Nanoparticles Stabilized by Collagen and Their Application in Catalytic Reduction of 4-Nitrophenol. *Chem. Lett.* **2008**, *37*, 834–835.
(38) Schurer, J. W.; Kalicharan, D.; Hoedemaeker, P. J.; Molenaar, I. The Use of Polyethyleneimine for Demonstration of Anionic Sites in Basement Membranes and Collagen Fibrils. *J. Histochem. Cytochem.* **1978**, *26*, 688–689.
(39) Sebag, J.; Balazs, E. A. Morphology and Ultrastructure of Human Vitreous Fibers. *Invest. Ophthalmol. Vis. Sci.* **1989**, *30*, 1867–1871.
(40) Hleb, E. Y.; Lapotko, D. O. Photothermal Properties of Gold Nanoparticles under Exposure to High Optical Energies. *Nanotechnology* **2008**, *19*, 355702.
(41) Lapotko, D. Pulsed Photothermal Heating of the Media during Bubble Generation around Gold Nanoparticles. *Int. J. Heat Mass Transf.* **2009**, *52*, 1540–1543.

(42) Riggins, J.; Pedrotti, L. S.; Keates, R. H. Evaluation of the Neodymium-YAG Laser for Treatment of Ocular Opacities. *Ophthalmic Surg. Lasers Imaging Retina* **1983**, *14*, 675–682.
(43) Prow, T. W. Toxicity of Nanomaterials to the Eye. *Wiley Interdiscip. Rev. Nanomed. Nanobiotechnol.* **2010**, *2*, 317–333.
(44) Kim, J. H.; Kim, J. H.; Kim, K.-W.; Kim, M. H.; Yu, Y. S. Intravenously Administered Gold Nanoparticles Pass through the Blood-Retinal Barrier Depending on the Particle Size, and Induce No Retinal Toxicity. *Nanotechnology* **2009**, *20*, 505101.
(45) Bakri, S. J.; Pulido, J. S.; Mukherjee, P.; Marler, R. J.; Mukhopadhyay, D. Absence of Histologic Retinal Toxicity of Intravitreal Nanogold in a Rabbit Model. *Retina Phila. Pa* **2008**, *28*, 147–149.
(46) Masse, F.; Ouellette, M.; Lamoureux, G.; Boisselier, E. Gold Nanoparticles in Ophthalmology. *Med. Res. Rev.* **2019**, *39*, 302–327.
(47) Hutton-Smith, L. A.; Gaffney, E. A.; Byrne, H. M.; Maini, P. K.; Schwab, D.; Mazer, N. A. A Mechanistic Model of the Intravitreal Pharmacokinetics of Large Molecules and the Pharmacodynamic Suppression of Ocular Vascular Endothelial Growth Factor Levels by Ranibizumab in Patients with Neovascular Age-Related Macular Degeneration. *Mol. Pharm.* **2016**, *13*, 2941–2950.
(48) Palanker, D. Femtosecond Lasers for Ophthalmic Surgery Enabled by Chirped-Pulse Amplification. *N. Engl. J. Med.* **2018**, *379*, 2267–2269.
(49) Turkevich, J.; Stevenson, P. C.; Hillier, J. A Study of the Nucleation and Growth Processes in the Synthesis of Colloidal Gold. *Discuss. Faraday Soc.* **1951**, *11*, 55.
(50) Haiss, W.; Thanh, N. T. K.; Aveyard, J.; Fernig, D. G. Determination of Size and Concentration of Gold Nanoparticles from UV−Vis Spectra. *Anal. Chem.* **2007**, *79*, 4215–4221.
(51) Xu, Y.; Gustafson, B. Å. S. A Generalized Multiparticle Mie-Solution: Further Experimental Verification. *J. Quant. Spectrosc. Radiat. Transf.* **2001**, *70*, 395–419.
(52) Bohren, C. F.; Huffman, D. R. *Absorption and Scattering of Light by Small Particles*; 1983.
(53) Xu, Y.; Wang, R. T. Electromagnetic Scattering by an Aggregate of Spheres: Theoretical and Experimental Study of the Amplitude Scattering Matrix. *Phys. Rev. E* **1998**, *58*, 3931–3948.
(54) *Handbook of Optical Constants of Solids II*; Palik, E. D., Ed.; Academic Press: Boston, 1991.
(55) Chettiar, U. K.; Engheta, N. Internal Homogenization: Effective Permittivity of a Coated Sphere. *Opt. Express* **2012**, *20*, 22976–22986.
(56) Leonard, D. W.; Meek, K. M. Refractive Indices of the Collagen Fibrils and Extrafibrillar Material of the Corneal Stroma. *Biophys. J.* **1997**, *72*, 1382–1387.
(57) Sebag, J.; Yee, K. M. P.; Wa, C. A.; Huang, L. C.; Sadun, A. A. Vitrectomy for Floaters: Prospective Efficacy Analyses and Retrospective Safety Profile. *Retina Phila. Pa* **2014**, *34*, 1062–1068.
(58) Rostami, B.; Nguyen-Cuu, J.; Brown, G.; Brown, M.; Sadun, A. A.; Sebag, J. Cost Effectiveness of Limited Vitrectomy for Vision Degrading Myodesopsia. *Am. J. Ophthalmol.* **2019**.
(59) Braeckmans, K.; Remaut, K.; Vandenbroucke, R. E.; Lucas, B.; De Smedt, S. C.; Demeester, J. Line FRAP with the Confocal Laser Scanning Microscope for Diffusion Measurements in Small Regions of 3-D Samples. *Biophys. J.* **2007**, *92*, 2172–2183.
(60) Mazza, D.; Braeckmans, K.; Cella, F.; Testa, I.; Vercauteren, D.; Demeester, J.; De Smedt, S. S.; Diaspro, A. A New FRAP/FRAPa Method for Three-Dimensional Diffusion Measurements Based on Multiphoton Excitation Microscopy. *Biophys. J.* **2008**, *95*, 3457–3469.

(61) Deschout, H.; Raemdonck, K.; Demeester, J.; Smedt, S. C. D.; Braeckmans, K. FRAP in Pharmaceutical Research: Practical Guidelines and Applications in Drug Delivery. *Pharm. Res.* **2014**, *31*, 255–270.
(62) Xiong, R.; Vandenbroucke, R. E.; Broos, K.; Brans, T.; Wonterghem, E. V.; Libert, C.; Demeester, J.; Smedt, S. C. D.; Braeckmans, K. Sizing Nanomaterials in Bio-Fluids by CFRAP Enables Protein Aggregation Measurements and Diagnosis of Bio-Barrier Permeability. *Nat. Commun.* **2016**, *7*, 12982.
(63) González-Rubio, G.; Guerrero-Martínez, A.; Liz-Marzán, L. M. Reshaping, Fragmentation, and Assembly of Gold Nanoparticles Assisted by Pulse Lasers. *Acc. Chem. Res.* **2016**, *49*, 678–686.
(64) Lorén, N.; Hagman, J.; Jonasson, J. K.; Deschout, H.; Bernin, D.; Cella-Zanacchi, F.; Diaspro, A.; McNally, J. G.; Ameloot, M.; Smisdom, N.; Nydén, M.; Hermansson, A.-M.; Rudemo, M.; Braeckmans, K. Fluorescence Recovery after Photobleaching in Material and Life Sciences: Putting Theory into Practice. *Q. Rev. Biophys.* **2015**, *48*, 323–387.
(65) Liu, J.; Xiong, R.; Brans, T.; Lippens, S.; Parthoens, E.; Zanacchi, F. C.; Magrassi, R.; Singh, S. K.; Kurungot, S.; Szunerits, S.; Bové, H.; Ameloot, M.; Fraire, J. C.; Teirlinck, E.; Samal, S. K.; Rycke, R. D.; Houthaeve, G.; Smedt, S. C. D.; Boukherroub, R.; Braeckmans, K. Repeated Photoporation with Graphene Quantum Dots Enables Homogeneous Labeling of Live Cells with Extrinsic Markers for Fluorescence Microscopy. *Light Sci. Appl.* **2018**, *7*, 47.
(66) Ciapetti, G.; Cenni, E.; Pratelli, L.; Pizzoferrato, A. *In Vitro* Evaluation of Cell/Biomaterial Interaction by MTT Assay. *Biomaterials* **1993**, *14*, 359–364.